

COMMUNICATIONS

High Resolution MAS-NMR of Quadrupolar Nuclei in Powders

A. SAMOSON, E. KUNDLA, AND E. LIPPMAA

*Department of Physics, Institute of Chemical Physics and Biophysics
of the Estonian Academy of Sciences, Tallinn 200001, USSR*

Received March 4, 1982

Interest in high-resolution NMR of quadrupolar nuclei in solids has grown considerably during the past year (1-4). In this study we want to show the possibilities and limitations of magic-angle spinning (MAS) in high-resolution NMR of quadrupolar nuclei in solids with special emphasis on quadrupolar nuclei with half-integer spin. It is well known that fast sample spinning can effectively average randomly oriented spin-interaction tensors. This property of MAS leads to a substantial line narrowing not only in the case of first-order perturbation effects, but also in the presence of contributions from second-order perturbations to the Zeeman interaction.

In our approximation, evolution of the state of a spin system in an external magnetic field is governed by the usual Hamiltonian

$$\mathcal{H} = \mathcal{H}_Z + \mathcal{H}_Q + \mathcal{H}_{CS} + \mathcal{H}_D. \quad [1]$$

In a strong magnetic field B_0 , the Zeeman term predominates over the quadrupole \mathcal{H}_Q , chemical shift \mathcal{H}_{CS} , and dipolar \mathcal{H}_D terms in the Hamiltonian

$$|\mathcal{H}_Z| \gg |\mathcal{H}_Q|, |\mathcal{H}_{CS}|, |\mathcal{H}_D| \quad [2]$$

and it is reasonable to use the interaction representation

$$\tilde{\mathcal{H}} = e^{i\mathcal{H}_Z t} \mathcal{H} e^{-i\mathcal{H}_Z t} \quad [3]$$

and to form an average Hamiltonian in the first approximation over the Larmor period, while considering the time dependence due to sample spinning at the much lower frequency ω_r as parametric. In many samples the dipolar interactions between quadrupolar nuclei are rather weak due to dilution, and heteronuclear dipolar couplings with the abundant nuclei can be effectively removed by rf decoupling, which means that one can neglect \mathcal{H}_D in [1]. This leads to considerable simplification of [1], since we can express it just for one spin I . Isotropic chemical shift σ_{iso} of the quadrupolar nucleus I is included in the Zeeman term

$$\mathcal{H}_Z = -\gamma(1 - \sigma_{iso})B_0 I_0 \equiv \omega_L I_0. \quad [4]$$

If additionally

$$|\mathcal{H}_Q| \gg |\mathcal{H}_{\text{CSA}}|, \quad [5]$$

the effective Hamiltonian can be confined to three terms

$$\begin{aligned} \mathcal{H}_{\text{eff}} = & \frac{\omega_L}{2\pi} \int_0^{2\pi/\omega_L} \tilde{\mathcal{H}}_Q(t) dt + \frac{\omega_L}{2\pi} \int_0^{2\pi/\omega_L} \tilde{\mathcal{H}}_{\text{CSA}}(t) dt \\ & - i \frac{\omega_L}{4\pi} \int_0^{2\pi/\omega_L} dt \int_0^t [\tilde{\mathcal{H}}_Q(t), \tilde{\mathcal{H}}_Q(t')] dt' = \tilde{\mathcal{H}}_Q^{(0)} + \tilde{\mathcal{H}}_{\text{CSA}}^{(0)} + \tilde{\mathcal{H}}_Q^{(1)}, \quad [6] \end{aligned}$$

where

$$\tilde{\mathcal{H}}_Q^{(0)} = \frac{eQ}{4I(2I-1)\hbar} \sqrt{2/3} V_{20}^Q (3I_0^2 - I^2),$$

$$\tilde{\mathcal{H}}_{\text{CSA}}^{(0)} = \gamma B_0 \sqrt{2/3} V_{20}^{\text{CSA}} I_0,$$

$$\begin{aligned} \tilde{\mathcal{H}}_Q^{(1)} = & \left[\frac{eQ}{4I(2I-1)\hbar} \right]^2 \frac{1}{\omega_L} \times [2|V_{21}^Q|^2(4I^2 - 2I_0^2 - 1)I_0 + 2|V_{22}^Q|^2(2I^2 - 2I_0^2 - 1)I_0 \\ & + \sqrt{6}V_{20}^Q V_{2-1}^Q(4I_0^2 - 4I_0 + 1)I_+ - \sqrt{6}V_{20}^Q V_{21}^Q(4I_0^2 + 4I_0 + 1)I_- \\ & + 2\sqrt{6}V_{20}^Q V_{2-2}^Q(I_0 - 1)I_+^2 + 2\sqrt{6}V_{20}^Q V_{22}^Q(I_0 + 1)I_-^2]. \end{aligned}$$

The interaction tensor components V_{2j}^λ are expressed through the Wigner rotation matrices (e.g., 5)

$$V_{2j}^\lambda = \sum_{m'} \mathcal{D}_{m'j}^{(2)}(\omega, t, \arccos(1/\sqrt{3}), 0) \sum_{m''} \mathcal{D}_{m''m'}^{(2)}(\alpha^\lambda, \beta^\lambda, \gamma^\lambda) \rho_{2m''}^\lambda.$$

The Eulerian angles $\alpha^\lambda, \beta^\lambda, \gamma^\lambda$ ($\omega, t, \arccos(1/\sqrt{3}), 0$) express the orientation of the spinner frame (laboratory frame) in the principal axes system of the interaction tensor $\lambda = \text{CSA}$ or Q (spinner frame). The relevant principal values are

$$\rho_{20}^{\text{CSA}} = \sqrt{2/3} \Delta\sigma; \quad \rho_{22}^{\text{CSA}} \equiv \rho_{2\pm 2}^{\text{CSA}} = -1/3 \Delta\sigma \eta_\sigma,$$

$$\rho_{20}^Q = \sqrt{3/2} eQ; \quad \rho_{22}^Q \equiv \rho_{2\pm 2}^Q = 1/2 eQ \eta_Q,$$

where the asymmetry parameters η_σ and η_Q refer to chemical shift anisotropy and quadrupole interactions, respectively.

To a good approximation, \mathcal{H}_{eff} can be regarded as diagonal in the basis of I_0 eigenfunctions $|m\rangle$. The nondiagonal elements are either zero or smaller than the difference between the corresponding diagonal elements by at least the factor $eQV_{2j}^Q/\hbar\omega_L$ throughout the whole rotation period.

The resonance frequency in the rotating frame of an arbitrary single quantum transition of the spin I can be expressed as

$$\begin{aligned} \omega_{m,m-1} = & \langle m | \mathcal{H}_{\text{eff}} | m \rangle - \langle m-1 | \mathcal{H}_{\text{eff}} | m-1 \rangle \\ = & \omega_{m,m-1}^0 + \sum_{n=1}^4 [A_n \cos(n\omega_r t) + B_n \sin(n\omega_r t)], \quad [7] \end{aligned}$$

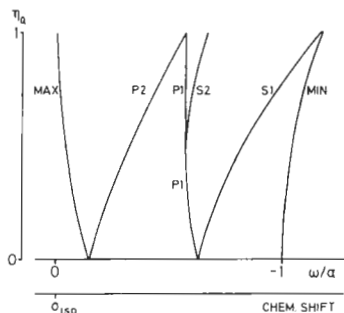


FIG. 1. The positions of singularities, described by Eq. [8], as functions of the electric field gradient asymmetry parameter η_Q , in the lineshape of the centerband of the central $\pm 1/2 \leftrightarrow \mp 1/2$ transition of a half-integer spin. The isotropic chemical shielding σ_{150} of the quadrupole nucleus is taken as the zero point for the lineshape functions.

where

$$\omega_{m,m-1}^0 = -a \left[1 + \frac{\eta_Q^2}{3} - \frac{6I(I+1) - 34m(m-1) - 13}{2I(I+1) - 14m(m-1) - 5} f(\alpha^Q, \beta^Q) \right] \quad [8]$$

$$a = \sqrt[3]{\frac{(e^2qQ/\hbar)^2}{\omega_L} \frac{2I(I+1) - 14m(m-1) - 5}{I^2(2I-1)^2}}$$

$$f(\alpha^Q, \beta^Q) = \sin^2 \beta^Q (1 - \frac{7}{8} \sin^2 \beta^Q) - \frac{1}{6} \eta_Q \sin^2 \beta^Q (3 - \frac{7}{2} \sin^2 \beta^Q) \\ \times \cos^2 \alpha^Q + \frac{1}{18} \eta_Q^2 [1 + \sin^2 \beta^Q (1 - \frac{7}{4} \cos^2 2\alpha^Q)].$$

Explicit forms of the frequency modulation parameters A_n and B_n are given in the Appendix. These modulation parameters are numerically of the order of $|\mathcal{H}_Q + \mathcal{H}_{CSA}|$.

If condition [2] is partially violated ($|\mathcal{H}_Z| < 10|\mathcal{H}_Q|$), further improvement could be provided with the inclusion of additional expansion terms in the average Hamiltonian [6] and subsequent diagonalization of \mathcal{H}_{eff} . The rotation-produced time dependence is still treated as parametric and can be taken into account only in the last step during calculation of the line positions and intensities of every crystallite in the sample. The central line of every crystallite and every possible transition lies at the average frequency so calculated.

According to [7], every individual crystallite in the powder sample creates a central line at the frequency $\omega_{m,m-1}^0$ and numerous lines spaced by $\pm k\omega_r$, $k = 1, 2, \dots$, from it as sidebands, with amplitudes depending upon the ratios $A_n/n\omega_r$ and $B_n/n\omega_r$. If the deviation of the central line frequency due to various crystallite orientations is smaller than ω_r , then the powder pattern centerband and the spinning sidebands, both of which feature complicated lineshapes, do not overlap.

In the $\omega_r \gg A_n, B_n$ limit, the centerband lineshape is determined by $\omega_{m,m-1}^0$. This can be the case for the central $\pm 1/2 \leftrightarrow \mp 1/2$ transition of a half-integer spin. Assuming random distribution of crystallites in the powder sample, the lineshape of this transition can be calculated. As shown in Fig. 1, this lineshape features two peaks, $\omega_{P1} = -(\frac{5}{8} - \frac{1}{4}\eta_Q + \frac{7}{24}\eta_Q^2)a$ for $0 \leq \eta_Q \leq \frac{3}{7}$, or $-\frac{4}{7}a$ for $\frac{3}{7} \leq \eta_Q \leq 1$, ω_{P2}

$= -\frac{1}{7}(1 + \eta_Q)^2 a$ for $0 \leq \eta_Q \leq 1$, and one or two shoulders, $\omega_{S1} = -(\frac{5}{8} + \frac{1}{4}\eta_Q + \frac{7}{24}\eta_Q^2)a$ for $0 \leq \eta_Q \leq 1$, $\omega_{S2} = -(\frac{5}{8} - \frac{1}{4}\eta_Q + \frac{7}{24}\eta_Q^2)a$ for $\frac{3}{7} \leq \eta_Q \leq 1$, between the flanks at $\omega_{MIN} = -(1 + \frac{1}{6}\eta_Q^2)a$ and $\omega_{MAX} = -\frac{1}{7}(1 - \eta_Q^2)a$.

In the case of axial symmetry $\eta_Q = 0$, the half-integer spin central transition centerband lineshape can be expressed analytically. The line intensity $J(\omega_{1/2, -1/2}^0)$ as a function of frequency is equal to $J_+(\omega) + J_-(\omega)$ for $-\frac{1}{7}a \geq \omega \geq \frac{5}{8}a$, or $J_+(\omega)$ for $-\frac{5}{8}a > \omega \geq -a$, where $J_{\pm}(\omega) = [(\sqrt{27/56} \pm \sqrt{-1/7 - \omega/a})(-1/7 - \omega/a)]^{-1/2}$. The center of gravity (ω_c) of this complicated lineshape is shifted from the Larmor frequency, which includes the isotropic chemical shift, and lies at $\omega_c = -(\frac{2}{5})a$.

A slightly different value results for this shift if one uses for the effective Hamiltonian the zeroth-order average over the rotation period of $\tilde{\mathcal{H}}_Q^{(0)} + \tilde{\mathcal{H}}_Q^{(1)}$. The result, however, is not readily applicable because when $|\tilde{\mathcal{H}}_Q^{(0)}| > \omega$, which is practically

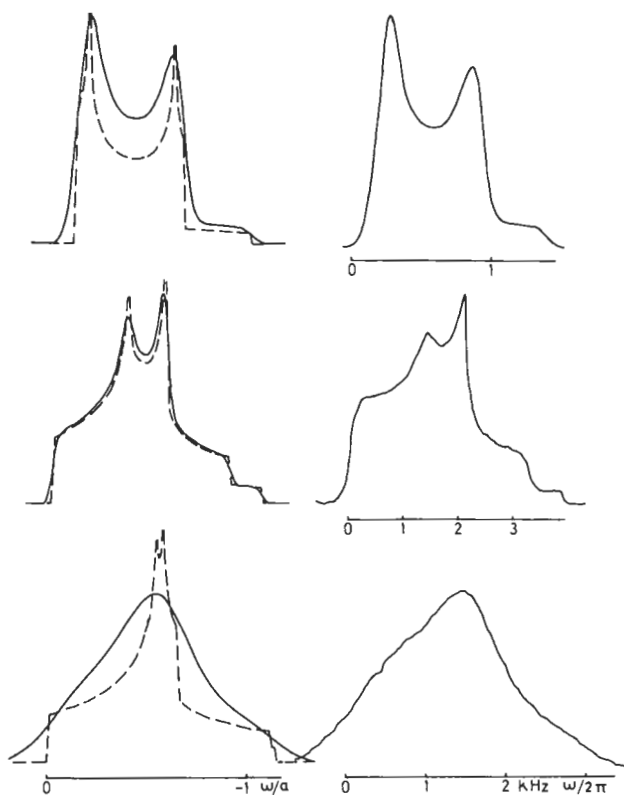


FIG. 2. Numerically calculated and experimental powder pattern lineshapes of the central $\pm\frac{1}{2} \leftrightarrow \mp\frac{3}{2}$ transition of half-integer spins in the fast rotation limit. Left: dashed lines, calculated from Eq. [8]; solid lines, with additional Gaussian broadening. Right: experimental spectra. All spectra were recorded on a Bruker-Physik CXP-200 spectrometer with rapid (ω , > 4 kHz) sample spinning. The spectrometer computer (Aspect-2000) was used for numerical calculations using a program written in Pascal. Upper: ^{23}Na ($I = \frac{3}{2}$) in solid sodium nitrite NaNO_2 , $e^2qQ/h = 1.10$ MHz, $\eta_Q = 0.109$ (9). Middle: ^{23}Na ($I = \frac{3}{2}$) in natrolite $e^2qQ/h = 1.76$ MHz, $\eta_Q = 0.643$ (10). Lower: ^{27}Al ($I = \frac{5}{2}$) in spodumene $e^2qQ/h = 2.95$ MHz, $\eta_Q = 0.94$ (4).

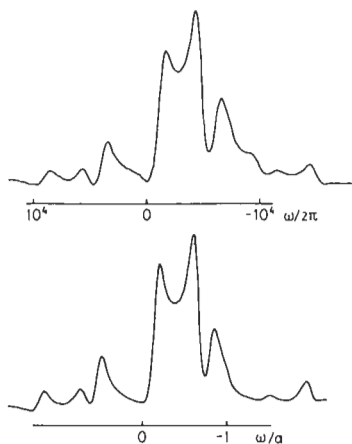


FIG. 3. Numerically calculated (upper) and experimental (lower) MAS-NMR spectra of ^{11}B ($I = \frac{3}{2}$) in solid B_2O_3 . Both the centerband and first two sidebands of the central $\pm\frac{1}{2} \leftrightarrow \mp\frac{1}{2}$ transition are included. Only quadrupolar interactions were taken into account in calculating the A_n values. $e^2qQ/h = 2.76$ MHz, $\eta_Q = 0$, $\omega_r = 4.9$ kHz (12).

always the case, the higher-order terms of the Hamiltonian, averaged over the rotation period, tend to diverge (6).

For clarity, the discussion is separated into three main cases.

(1) $\omega_r \gg A_n, B_n$. Centerband lineshapes of the central transition, numerically calculated using Eq. [8] and averaged over all possible values of the Eulerian angles α^Q and β^Q , are shown in Fig. 2 for various values of the asymmetry parameter η_Q , and compared with the relevant experimental lineshapes. In the absence of additional homogeneous line broadening, a rather good fit is observed. Some additional line broadening, possibly due to chemical inhomogeneity, is present in the ^{27}Al spectrum of spodumene. Experimental data show that the positions of lineshape singularities remain unchanged at various sample rotation rates as long as the centerband remains separated from the sidebands.

(2) $\omega_r \approx A_n, B_n$. In the case of axial symmetry of the quadrupole interaction, the influence of sideband formation, and thus of the actual values of A_n and B_n , can relatively easily be taken into account. The corresponding theoretical spectrum, numerically calculated to show the first and second sidebands, is compared with the experimental spectrum in Fig. 3. The fit is convincing, and lacks only some contribution in the first sidebands from the neglected dipolar and CSA interactions.

(3) $\omega_r \ll A_n, B_n$. The observation of noncentral transitions of a half-integer spin, for example, of the $\pm\frac{3}{2} \leftrightarrow \pm\frac{1}{2}$ transitions, is difficult in most cases because $A_n, B_n \gg \omega_r$ due to a large contribution from the $\mathcal{H}_Q^{(0)}$ term. If one tries to record other transitions together with the central $\pm\frac{1}{2} \leftrightarrow \mp\frac{1}{2}$ transition, the resulting centerband intensities of these transitions are greatly reduced due to the formation of a large number of sidebands, coupled with insufficient excitation efficiency caused by the large excitation frequency offsets in most crystallites during sample spinning. It was, however, possible to register the frequency shift between the central $\pm\frac{1}{2} \leftrightarrow \mp\frac{1}{2}$ and coincident $\pm\frac{3}{2} \leftrightarrow \pm\frac{1}{2}$ transitions of an $I = \frac{3}{2}$ spin by using the first

sidebands for which the signal intensities are more nearly equal. Such sideband spectra of ^{23}Na spins in NaNO_3 are shown in Fig. 4. It follows from Eq. [7] that the peaks of maximum intensity in the first sidebands must be separated by 95 to 220 Hz, a prediction well borne out in experiment.

It must be mentioned that to observe transitions with large contributions from $\bar{\nu}_Q^{(0)}$ to the resonance frequency, an extremely precise setting of the magic angle is needed during sample spinning, as was pointed out by Ackerman (7) and Alla (8).

The results show that high-resolution MAS-NMR of quadrupolar nuclei with half-integer spins in powder samples will be a valuable tool in the study of solids, providing information about the isotropic chemical shifts and the quadrupolar interaction constants. The necessary condition

$$\omega_r > \omega_{\text{MAX}} - \omega_{\text{MIN}} \approx a$$

is easily met for many common nuclei, in particular for ^{11}B , ^{23}Na , and ^{27}Al . Since these nuclei are not particularly abundant and are nearly always separated by other nuclei in chemical compounds, the weak dipolar interactions are averaged out by the rapid magic-angle sample spinning, and about an order of magnitude line narrowing results, providing very characteristic and easily interpreted lineshapes in the spectra.

APPENDIX

$$A_n = \sum_{\lambda} C^{\lambda} [A_n^{\lambda} \cos(n\gamma^{\lambda}) + B_n^{\lambda} \sin(n\gamma^{\lambda})],$$

$$B_n = \sum_{\lambda} C^{\lambda} [B_n^{\lambda} \cos(n\gamma^{\lambda}) - A_n^{\lambda} \sin(n\gamma^{\lambda})],$$

where $\lambda = \text{CSA}, Q(0), Q(1)$ and

$$C^{\text{CSA}} = \sqrt{2/3} \gamma B_0,$$

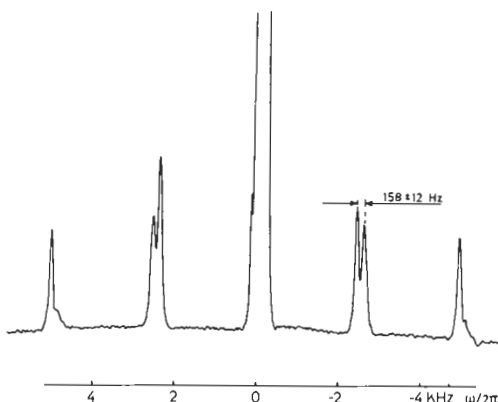


FIG. 4. Experimental NMR-MAS powder spectra of ^{23}Na ($I = 3/2$) in sodium nitrate NaNO_3 . The spinning sidebands contain information about the frequency shift between the $\pm 1/2 \leftrightarrow \pm 1/2$ and $\pm 1/2 \leftrightarrow \mp 1/2$ transitions. $e^2qQ/h = 0.334$ MHz, $\eta_Q = 0$ (13).

$$C^{Q(0)} = \frac{eQ}{4I(2I-1)\hbar} \sqrt{6}(2m-1),$$

$$C^{Q(1)} = \left[\frac{eQ}{4I(2I-1)\hbar} \right]^2 \frac{1}{\omega_L}.$$

For $\lambda = \text{CSA}$ and $Q(0)$

$$A_1^\lambda = -\frac{\sqrt{2}}{2} \sin^2 \beta^\lambda \rho_{20}^\lambda + \frac{\sqrt{3}}{3} \cos 2\alpha^\lambda \sin 2\beta^\lambda \rho_{22}^\lambda,$$

$$A_2^\lambda = \frac{1}{2} \sin 2\beta^\lambda \rho_{20}^\lambda + \frac{\sqrt{6}}{6} \cos 2\alpha^\lambda (1 + \cos^2 \beta^\lambda) \rho_{22}^\lambda,$$

$$B_1^\lambda = -\frac{2\sqrt{3}}{3} \sin 2\alpha^\lambda \sin \beta^\lambda \rho_{22}^\lambda,$$

$$B_2^\lambda = -\frac{\sqrt{6}}{3} \sin 2\alpha^\lambda \cos \beta^\lambda \rho_{22}^\lambda,$$

$$A_3^\lambda = A_4^\lambda = B_3^\lambda = B_4^\lambda = 0.$$

For $\lambda = Q(1)$

$$A_1^\lambda = -\sin 2\beta \left[\frac{\sqrt{2}}{9} \left(\cos^2 2\alpha \frac{1 + \cos^2 \beta}{2} + \sin^2 2\alpha \right) (M_1 + \frac{1}{2} M_2) \right. \\ \left. + \frac{\sqrt{2}}{6} \cos^2 2\alpha \sin^2 \beta (M_1 + M_2) \right] \rho_{22}^2 + \cos 2\alpha \sin 2\beta \left[\frac{\sqrt{3}}{9} \cos^2 \beta (M_1 + \frac{1}{2} M_2) \right. \\ \left. + \frac{\sqrt{3}}{18} (1 - 3 \cos 2\beta) (M_1 + M_2) \right] \rho_{22} \rho_{20} + \frac{\sqrt{2}}{12} \sin 2\beta [\sin^2 \beta (M_1 + \frac{1}{2} M_2) \\ + (3 \cos^2 \beta - 1) (M_1 + M_2)] \rho_{20}^2,$$

$$A_2^\lambda = \sin^2 \beta \left[\frac{1}{3} \cos^2 2\alpha (1 + \cos^2 \beta) (M_1 + M_2) + \frac{1}{6} (\cos^2 2\alpha \cos^2 \beta - \sin^2 2\alpha) \right. \\ \left. \times (M_1 - 2M_2) \right] \rho_{22}^2 + \cos 2\alpha \left[\frac{\sqrt{6}}{18} (3 \sin^4 \beta + 3 \cos^4 \beta + 2 \cos^2 \beta - 1) \right. \\ \left. \times (M_1 + M_2) - \frac{\sqrt{6}}{36} \sin^2 2\beta (M_1 - 2M_2) \right] \rho_{22} \rho_{20} + \frac{1}{6} \sin^2 \beta [(3 \cos^2 \beta - 1) \\ (M_1 + M_2) + \cos^2 \beta (M_1 - 2M_2)] \rho_{20}^2,$$

$$A_3^\lambda = \sin 2\beta (4M_1 + M_2) \left[\frac{\sqrt{2}}{18} \left(\cos^2 2\alpha \frac{\cos^2 \beta + 1}{2} - \sin^2 2\alpha \right) \rho_{22}^2 \right. \\ \left. - \frac{\sqrt{3}}{18} \cos 2\alpha \cos^2 \beta \rho_{22} \rho_{20} - \frac{\sqrt{2}}{24} \sin^2 \beta \rho_{20}^2 \right],$$

$$A_4^\lambda = (4M_1 + M_2) \left[\frac{1}{72} (\cos^2 2\alpha (1 + \cos^2 \beta)^2 - 4 \sin^2 2\alpha \cos^2 \beta) \rho_{22}^2 \right. \\ \left. + \frac{\sqrt{6}}{72} \cos 2\alpha \sin^2 \beta (1 + \cos^2 \beta) \rho_{22} \rho_{20} + \frac{1}{48} \sin^4 \beta \rho_{20}^2 \right],$$

$$B_1^\lambda = \frac{\sqrt{2}}{36} \sin 4\alpha \sin^3 \beta (4M_1 + M_2) \rho_{22}^2 - \frac{\sqrt{3}}{9} \sin 2\alpha \sin \beta [(\cos^2 \beta + 1)(M_1 + \frac{5}{2}M_2) - (3 \cos^2 \beta - 1)(M_1 + M_2)] \rho_{22} \rho_{20},$$

$$B_2^\lambda = -\frac{1}{9} \sin 4\alpha \sin^2 \beta \cos \beta (4M_1 + M_2) \rho_{22}^2 + \frac{\sqrt{6}}{9} \sin 2\alpha \cos \beta [(1 - 3 \cos^2 \beta)(M_1 + M_2) + \sin^2 \beta (M_1 - 2M_2)] \rho_{22} \rho_{20},$$

$$B_3^\lambda = -\sin \beta (4M_1 + M_2) \left[\frac{\sqrt{2}}{36} \sin 4\alpha (3 \cos^2 \beta + 1) \rho_{22}^2 + \frac{\sqrt{3}}{18} \sin 2\alpha (1 - 3 \cos^2 \beta) \rho_{22} \rho_{20} \right],$$

$$B_4^\lambda = -\cos \beta (4M_1 + M_2) \left[\frac{1}{36} \sin 4\alpha (1 + \cos^2 \beta) \rho_{22}^2 + \frac{\sqrt{6}}{36} \sin 2\alpha \sin^2 \beta \rho_{22} \rho_{20} \right].$$

Here

$$\rho_{20} \equiv \rho^{Q(1)}, \quad \rho_{22} \equiv \rho_{22}^{Q(1)}, \quad \alpha, \beta, \gamma \equiv \alpha^{Q(1)}, \beta^{Q(1)}, \gamma^{Q(1)},$$

$$M_1 = 8I(I+1) - 48m(m-1) - 18,$$

$$M_2 = 4I(I+1) - 12m(m-1) - 6.$$

REFERENCES

1. E. KUNDLA, A. SAMOSON, AND E. LIPPMAN, *Chem. Phys. Lett.* **83**, 229 (1981).
2. A. SAMOSON AND E. KUNDLA, "Abstracts of the 5th Specialized Colloque AMPERE," p. 37, Uppsala, 1981.
3. D. I. BURTON AND R. K. HARRIS, private communication.
4. B. SCHNABEL, "Abstracts of the Schultagung: Moderne Methoden der Hochfrequenzspektroskopie," p. 35, Reinhardtbrunn, 1981.
5. H. W. SPIESS, in "NMR—Basic Principles and Progress" (P. Diehl, E. Fluck, and R. Kosfeld, Eds.), Vol. 15, p. 55, Springer-Verlag, Berlin/Heidelberg/New York, 1978.
6. M. MARICQ AND J. WAUGH, *J. Chem. Phys.* **70**, 3300 (1979).
7. J. L. ACKERMAN, R. ECKMAN, AND A. PINES, *Chem. Phys.* **42**, 423 (1979).
8. R. ECKMAN, M. ALLA, AND A. PINES, *J. Magn. Reson.* **41**, 440 (1980).
9. A. WEISS, *Z. Naturforsch. A* **15**, 536 (1960).
10. H. PETCH AND K. PENNINGTON, *J. Chem. Phys.* **36**, 1216 (1962).
11. H. E. PETCH, N. G. GRANNA, AND G. M. VOLKOFF, *Can. J. Phys.* **31**, 837 (1953).
12. A. H. SILVER AND P. J. BRAY, *J. Chem. Phys.* **29**, 984 (1958).
13. R. POUND, *Phys. Rev.* **79**, 685 (1950).